Electronic relaxation and vibrational dynamics in a thiophene oligomer studied under the same experimental condition with a sub-5 fs laser

2008 New J. Phys. 10 123021

(http://iopscience.iop.org/1367-2630/10/12/123021)

New Journal of Physics
The open-access journal for physics

Electronic relaxation and vibrational dynamics in a thiophene oligomer studied under the same experimental condition with a sub-5 fs laser

Zhuan Wang[1,2] **and Takayoshi Kobayashi**[1,2,3,4,5]

[1] Department of Applied Physics and Chemistry and Institute of Laser Science, University of Electro-Communications, Chofugaoka 1-5-1, Chofu, Tokyo 182-8585, Japan

[2] International Cooperative Research Project (ICORP), Japan Science and Technology Agency, 4-1-8 Honcho, Kawaguchi, Saitama 332-0012, Japan

[3] Institute of Laser Engineering, Osaka University, Yamadakami 2-6, Suita 565-0871, Ibaraki 567-0047, Japan

[4] Department of Electrophysics, National Chiao Tung University, 1001 Ta Hsueh Road, Hsinchu 3005, Taiwan

E-mail: kobayashi@ils.uec.ac.jp

New Journal of Physics **10** (2008) 123021 (13pp)
Received 28 May 2008
Published 16 December 2008
Online at http://www.njp.org/
doi:10.1088/1367-2630/10/12/123021

Abstract. Using a sub-5 fs pulse laser, the pump–probe experiment was performed on a quinoid thiophene derivative and both electronic relaxation and vibrational dynamics were clarified with the same experimental data. From the data, two population decay times of the lowest electronic excited state were determined to be 200 fs and 1.8 ps, which can be explained by the assumption that the 2^1A_g state lies below the exciton 1^1B_u state together with the very low fluorescence quantum efficiency. The relaxation process after excitation by the pump pulse was studied to be $1^1B_u \rightarrow 1^1B_u^* \rightarrow 2^1A_g \rightarrow 1^1A_g$. According to the experimental data, the location of the energy level was also discussed. The electronic dephasing time was determined to be 64 ± 4 fs by utilizing the data in the 'negative time' range. The vibrational dephasing time constant of the most strongly coupled mode with frequency of 1466 cm^{-1} was determined to be 520 ± 20 fs from the widths of the corresponding Fourier power spectra.

[5] Author to whom any correspondence should be addressed.

Contents

1. Introduction

Thiophene-based oligomers can readily be synthesized [1]–[3] with different numbers of monomer units ranging from two to twelve or more. Therefore, they can provide a series of conjugated systems with different π-electron delocalization lengths. Extensive theoretical and experimental studies have been conducted to better understand the basic physical properties of polythiophene, which has been one of the most frequently studied conjugated polymers since the 1990s [4]–[14]. They have been considered as promising materials from the viewpoint of application to optoelectronic devices [10], [15]–[18] such as light-emitting diodes and transistors [19]–[21].

Vibrational spectroscopy of polythiophenes has shown [11] they contain all-*s*-*trans* sequences of thiophene rings linked at α- and α'-positions with a distribution of conjugation length depending on both the sequential length and torsion angle of the thiophene ring. The distribution of conjugation lengths even within a group of the same oligomers has been ascribed to the existence of disordered structures in the polymer chain [22]. Polythiophene has a nondegenerate ground state like *cis*-polyacetylene has, which differs from the case for *trans*-polyacetylene, which has a degenerate ground state [4, 13]. In the case of conjugated polymers, there is only a very small number of examples with a degenerate ground state. The optical properties of doped polythiophene with a nondegenerate ground state have been discussed in terms of charged polarons and bipolarons [13]–[15], which are self-localized excitations in conjugated polymers. These nonlinear excitations are considered to be generated by the geometrical relaxation of the main-chain framework of the polymer. It is important to study the processes following the creation of an electron and hole by photoexcitation for better understanding of the mechanics of the generation of such nonlinear excitations.

It is also interesting to perform a comparative study between benzenoid thiophene and quinoid thiophene. This is because of the difference in the stable configurations in the ground and excited states between the two types of thiophenes. Benzenoid thiophene is expected to convert to 'quinoid' thiophene in the geometrical relaxation process, whereas quinoid thiophene is considered to relax to a 'benzenoid' structure because of the π–π^* transition. Here, we use quotation marks to indicate they do not have a typical quinoid or benzenoid structure but their structures have a substantial contribution from the quinoid or benzenoid configuration. Therefore, it is of great interest to study the ultrafast dynamics of the vibrational levels after the photoexcitation of quinoid thiophene, which has a quinoid structure in the ground

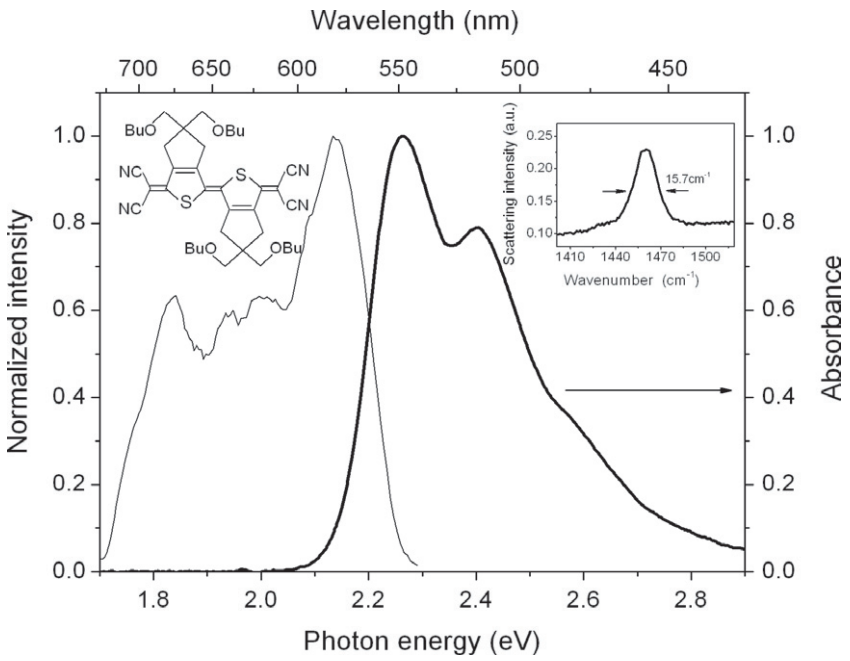

Figure 1. Laser (thin solid line) and absorption (thick solid line). The molecular structure of the quinoid thiophene derivative used in the present study was shown as inset. The measured Raman spectrum of this molecule excited at 488 nm was also shown as inset.

state. Ultrashort excited state dynamics of thiophene oligomers and polythiophene have been studied extensively [5, 12], [23]–[28], but all the studies were only on either the electronic relaxation or vibrational dynamics. Because of the inhomogeneity inevitable in such amorphous polymers, it is difficult to obtain samples having exactly the same properties. Even in the same sample, the properties can be substantially different depending on the probing position owing to the inhomogeneity introduced in the preparation process. For example, there are differences between the amorphous region and crystalline regions in the case of conjugated polymers. Therefore, it is also important to conduct an experiment probing the same position of the sample for the study of both dynamics. There is no reported study on electronic and vibrational dynamics for both dynamics being under the same conditions.

In this paper, femtosecond spectroscopy was performed with a quinoid thiophene derivative as a sample using a sub-5 fs ultrashort laser pulse. The population decay time of the electronic excited state, electronic phase and vibrational phase relaxation times were studied using the same probe-delay time-dependent absorbance change. This enables us to discuss the electronic relaxation and vibration dynamics under exactly the same experimental conditions, e.g. pump intensity and temperature.

2. Experiment

The sample quinoid thiophene derivative, hereafter abbreviated as Bx-2, has dicyanomethylene groups at the terminal position and is a highly amphoteric redox molecule; its molecular structure is shown in figure 1 [29]. The stationary absorption was recorded with an absorption

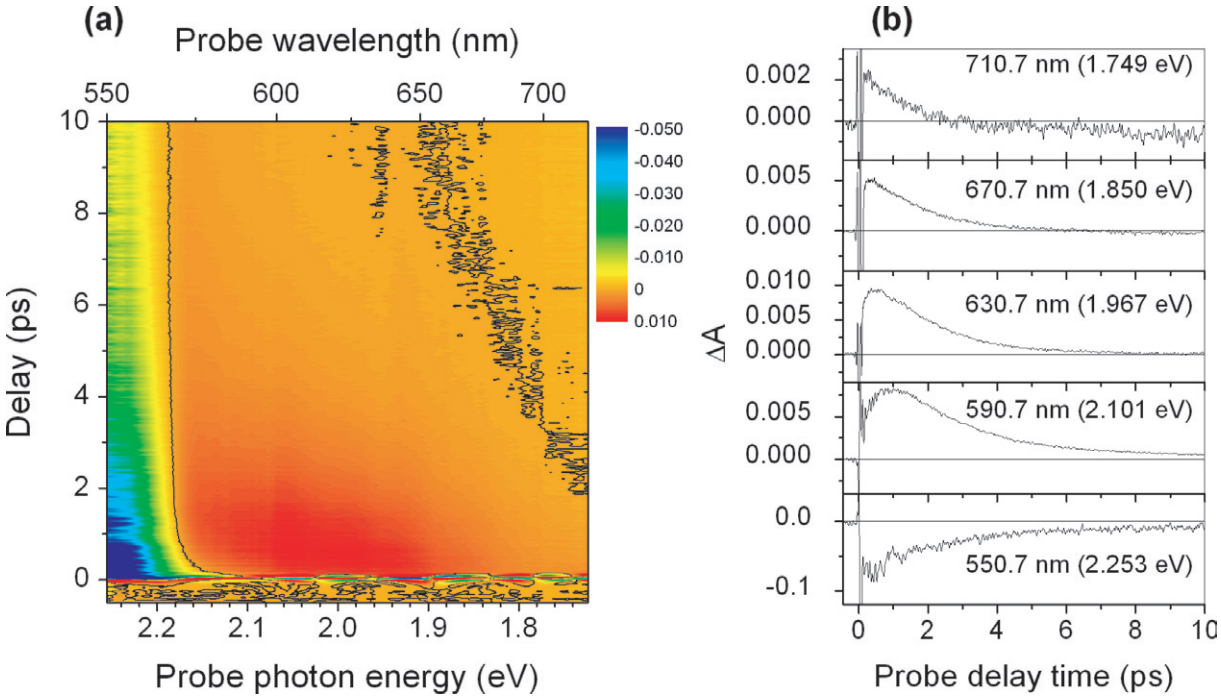

Figure 2. (a) Real-time spectrum ($\Delta A(\omega, t)$). The line in the figure shows the zero absorbance change. (b) Real-time traces at five different wavelengths.

spectrometer (Shimadzu, UV-3101PC) as shown in figure 1. The quinoid thiophene derivative was dissolved in tetrahydrofuran (THF) with a concentration of 0.02 wt%.

Pump and probe pulses were both produced from a noncollinear optical parametric amplifier (NOPA) seeded by a white-light continuum [30]–[32]. The pump source of this NOPA system was a regenerative amplifier (Spectra Physics, Spitfire) with operating parameters of 790 nm central wavelength, 50 fs pulse duration, 5 kHz repetition rate and 750 mW average output power. The spectrum of the output from the NOPA covered the spectral range of 545–735 nm. With the use of a compression system composed of a pair of prisms and a pair of chirped mirrors, the system supported a pulse with a pulse duration slightly shorter than 5 fs with constant spectral phase, indicating that the pulses were nearly Fourier-transform (FT) limited. The energy of the pump was ∼30 nJ, which corresponds to a photon density of 1.2×10^{15} photons cm^{-2}. The probe pulse energy was ∼6 nJ, five times weaker than the pump pulse. The transmission difference of the probe was dispersed by a polychromator (300 grooves mm^{-1}, 500 nm blazed) and then guided to avalanche photodetectors (APDs) by a 128-channel fiber bundle. The multichannel lock-in amplifier was designed for the purpose of detecting the signals simultaneously over the whole spectrum. The pump–probe signal was recorded with a delay time step of 10 fs in the time range from −0.5 to 20 ps. The entire experiment was performed at room temperature (293 ± 1 K).

3. Results and discussion

3.1. Two-dimensional difference absorption spectrum: electronic population relaxation

The two-dimensional difference absorption spectrum ($\Delta A(\omega, t)$) of Bx-2 excited by the sub-5 fs pulses from the NOPA is shown in figure 2(a). The real-time traces at five different probe photon

energies (wavelengths) are shown in figure 2(b). The figure shows that the electronic decay dynamics in the real-time traces seem to be rather complicated. In analyzing the data, it was assumed that the electronic decay functions after removing the highly oscillating vibrational contribution can be given by the following sum of three exponential functions with time constants τ_1, τ_2 and $\tau_3 \gg 20$ ps and amplitudes A'_1, A'_2 and A'_3 for all the channels.

$$\Delta A(t, \omega) = A'_1(\omega)\mathrm{e}^{-t/\tau_1} + A'_2(\omega)\mathrm{e}^{-t/\tau_2} + A'_3(\omega)\mathrm{e}^{-t/\tau_3}. \quad (1)$$

There are two reasons why the decay time traces were fitted with equation (1). Firstly, the values of the constants τ_1 and τ_2 depend on the probe photon energy (wavelength). The decay times τ_1 and τ_2 range 500–200 fs and 3.0–1.7 ps, respectively, over the entire probe spectral range. For example, τ_1 and τ_2 are 355 ± 4 fs and 2.8 ± 0.1 ps at a probe photon energy (wavelength) of 2.13 eV (582 nm), respectively, whereas they are 230 ± 20 fs and 1.7 ± 0.1 ps at 1.822 eV (681 nm). The difference between the short decay time τ_1 and long decay time τ_2 over the entire spectral range is as large as a factor of 5 and the width of the distribution function is smaller than a factor of about 2.5 in either case. Therefore, we consider a long decay and short decay as in equation (1). Secondly, even though τ_1 and τ_2 are not 'constant' in the probe photon energy (wavelength) range of observations, the wavelength dependences of both decay times are continuous with respect to wavelength. That is to say they change nearly monotonically with wavelength. Because of the continuous change, it is not possible to fit them even using more than five decay time 'constants'. Therefore, it is not meaningful to consider a greater number of decay times.

The decay dynamics function given by equation (1) can be modeled in two ways. One model is a sequential model (A) and the other is a parallel model (B), both of which are described in terms of states L_1, L_2, L_3 and G.

$$\text{(A)}\quad \mathrm{L_1} \xrightarrow{\tau_1} \mathrm{L_2} \xrightarrow{\tau_2} \mathrm{L_3} \xrightarrow{\tau_3 \gg 20\,\mathrm{ps}} \mathrm{G}$$

$$\text{(B)}\quad \mathrm{L_1} \xrightarrow{\tau_1} \mathrm{G}$$
$$\mathrm{L_2} \xrightarrow{\tau_2} \mathrm{G}$$
$$\mathrm{L_3} \xrightarrow{\tau_3 \gg 20\,\mathrm{ps}} \mathrm{G}.$$

Because the energy spacing in a molecule such as that studied in the present study is considered to be of the order of 1000 cm^{-1} or less due to the high state density, the sequential model can be concluded to be more feasible since the energy-gap law predicts much faster decay for $L_1 \rightarrow L_2$ or $L_2 \rightarrow L_3$ than for $L_1 \rightarrow L_3$, $L_1 \rightarrow G$ and $L_2 \rightarrow G$ [33]. In the following discussion, the sequential model is used. The results of the exponential fitting are plotted in figure 3. The following discussion on these two decay times uses the model shown in figure 4(a). A simple description is given for this model and then the decay times obtained in this study are discussed.

Oligothiophenes belong to the symmetry groups C_{2h} (2T, 4T, 6T) and C_{2v} (3T, 5T). The electronic ground state is $1A_g$ ($1A_1$ for C_{2v} symmetry) and the first two excited states are $1B_u$ ($1B_2$) and $2A_g$ ($2A_1$) as shown in figure 4(a). For small oligothiophenes, it is known that $1B_u$ lies below $2A_g$ with a tendency for the $1B_u$ energy to decrease more slowly than the $2A_g$ energy with an increase in the length of the polyenes to which oligothiophenes belong [34, 35].

The relaxation observed in the present study can be explained well by the assumption that the lowest excited state S_1 is the forbidden state 2^1A_g and the second lowest singlet state S_2

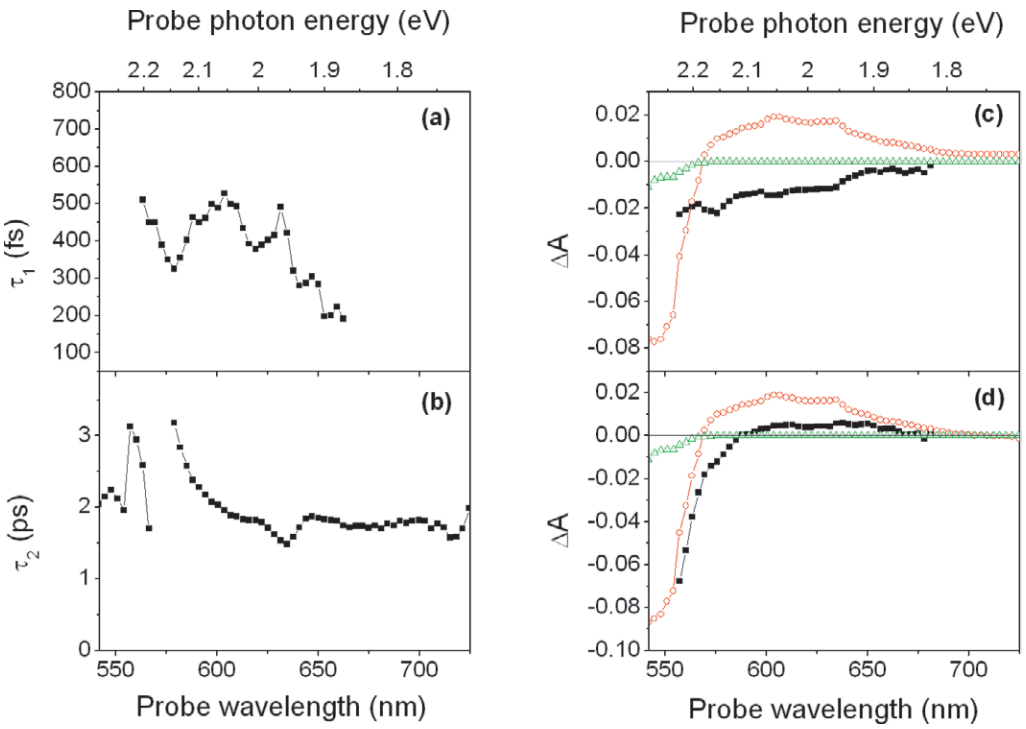

Figure 3. (a) and (b) the probe wavelength dependence of decay time of the exponential fitting to the real-time traces. (c) and (d) the coefficient spectra of the exponential fitting with parallel model and sequential model, respectively. Filled square, open circle and open triangle represent A'_1, A'_2, A'_3 and A_1, A_2, A_3, respectively in parts (c) and (d).

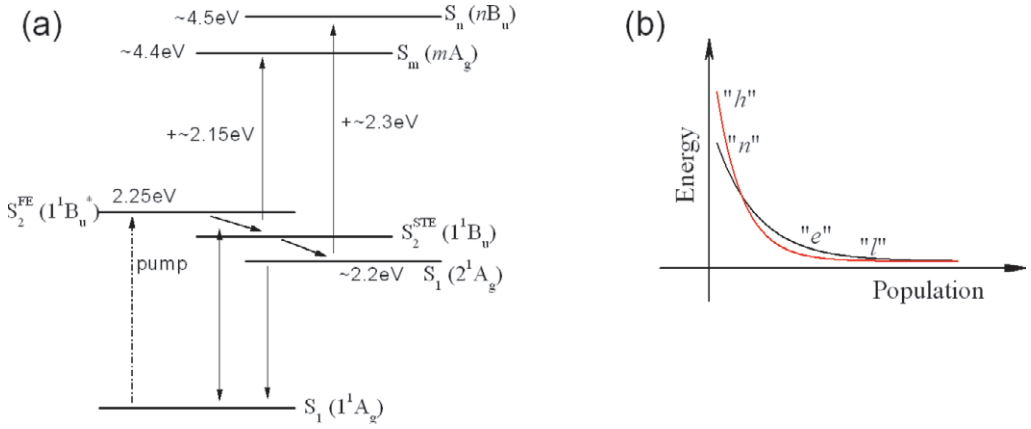

Figure 4. (a) Schematic of relaxation model of the studied molecule after photon excitation. S_0, electronic ground state; S_1, S_2, S_m and S_n, the electronic excited states. FE, free exciton; STE, self-trapped exciton. (b) Population distribution in the electronic state S_2^{STE}: relaxation takes place from the non-equilibrium state '*n*' (red line) to the equilibrium state '*e*' (black line). Population feeding occurs from the high-temperature hot levels '*h*' in the nonequilibrium state '*n*' to the low-temperature levels '*l*' in the equilibrium state '*e*'.

is the allowed state 1^1B_u. First, the quantum efficiency of the fluorescence was estimated to be smaller than 10^{-3}, which indicates the lowest state is the forbidden state. The properties of the experimental results for the decay times can then be explained well as follows. In the probe photon energy range 2.21–1.82 eV (wavelength range 560–680 nm), the shorter decay time (τ_1) gradually decreases from 600 to 200 fs. The 200 fs decay time was attributed to the relaxation from the free exciton (FE)$1^1B_u^*$ (S_2^{FE}) to the self-trapped exciton (STE) 1^1B_u (S_2^{STE}). The reason why τ_1 gradually increases with the probe photon energy is that during the relaxation process ($1^1B_u^* \rightarrow 1^1B_u$), the population of the lower vibrational levels of low vibrational modes is to be fed from higher vibrational levels as shown in figure 4(b). This induces a decay time for the transition from '*l*' to the higher electronic energy level longer than that from '*h*'. The decay time τ_2 has no obvious probe photon energy dependence and the averaged decay time was determined to be 1.8 ± 0.1 ps. This could be attributed to the time for relaxation from $S_2(1^1B_u)$ to $S_1(2^1A_g)$. Decay time τ_3, which is longer than 20 ps, reflects the relaxation process of $S_1 \rightarrow S_0$. The electronic dynamics observed and discussed above cannot be well explained by the model with the 2^1A_g state being the second lowest excited state and higher than the 1^1B_u exciton state. The quantitative explanation given below is applicable only to the model of S_2^{FE}, S_2^{STE} and S_1 being $1^1B_u^*$, 1^1B_u and 2^1A_g with 2^1A_g being lower than 1^1B_u.

In the sequential model supported by the energy-gap law, equation (1) can be rewritten using the spectra of L_1, L_2 and L_3:

$$\Delta A(t, \omega) = A_1(\omega)e^{-t/\tau_1} + A_2(\omega)(e^{-t/\tau_2} - e^{-t/\tau_1}) + A_3(\omega)(1 - e^{-t/\tau_2}), \tag{2}$$

with

$$\begin{aligned} A_1(\omega) &= A_1'(\omega) + A_2'(\omega) + A_3'(\omega), \\ A_2(\omega) &= A_2'(\omega) + A_3'(\omega), \\ A_3(\omega) &= A_3'(\omega). \end{aligned}$$

The calculated $A_1'(\omega)$, $A_2'(\omega)$ and $A_3'(\omega)$ and $A_1(\omega)$, $A_2(\omega)$ and $A_3(\omega)$ are shown in figures 3(c) and (d). Here, we used the values of τ_1 and τ_2 plotted in figures 3(a) and (b). Even though they are not constant over the entire probe spectral range, the deviation of the spectra shown in figures 3(c) and (d) is expected to be small. According to the assignment of the decay times τ_1, τ_2 and τ_3, the spectra $A_1(\omega)$, $A_2(\omega)$ and $A_3(\omega)$ are discussed as follows.

The spectra $A_1(\omega)$ and $A_2(\omega)$ have similar shape and negative and positive values in the shorter and longer wavelength ranges, respectively. The negative parts of $A_1(\omega)$ and $A_2(\omega)$ can be attributed to bleaching and/or stimulated emission and the positive part is due to the induced absorption from the excited state S_2^{FE} and S_2^{STE} to an even higher excited state $S_m(mA_g)$. The close similarity of $A_1(\omega)$ and $A_2(\omega)$ strongly supports the assignment of L_1 and L_2 as the FE state ($1^1B_u^*$) and STE (1^1B_u) with lifetimes of 200–600 fs.

As discussed above for the attribution of decay time τ_3, spectrum $A_3(\omega)$ is attributed to state $S_1(2^1A_g)$. However, as shown in figure 3(d), the $A_3(\omega)$ only has small negative values in the shorter wavelength range and is nearly zero in the longer wavelength range and has no obvious positive values in the probe spectral range. This could be explained as follows. (i) The state $S_1(2^1A_g)$ is lower than $S_2(1^1B_u)$ and the higher energy state $S_n(n\mathrm{Bu})$ is expected to be above $S_m(mA_g)$ [36], which indicates that the transition energy of $2^1A_g \rightarrow nB_u$ is greater than that of $1^1B_u \rightarrow mA_g$. Therefore, the induced absorption band is probably outside the present probe spectral range. (ii) The negative amplitude could be due to bleaching. It is considered

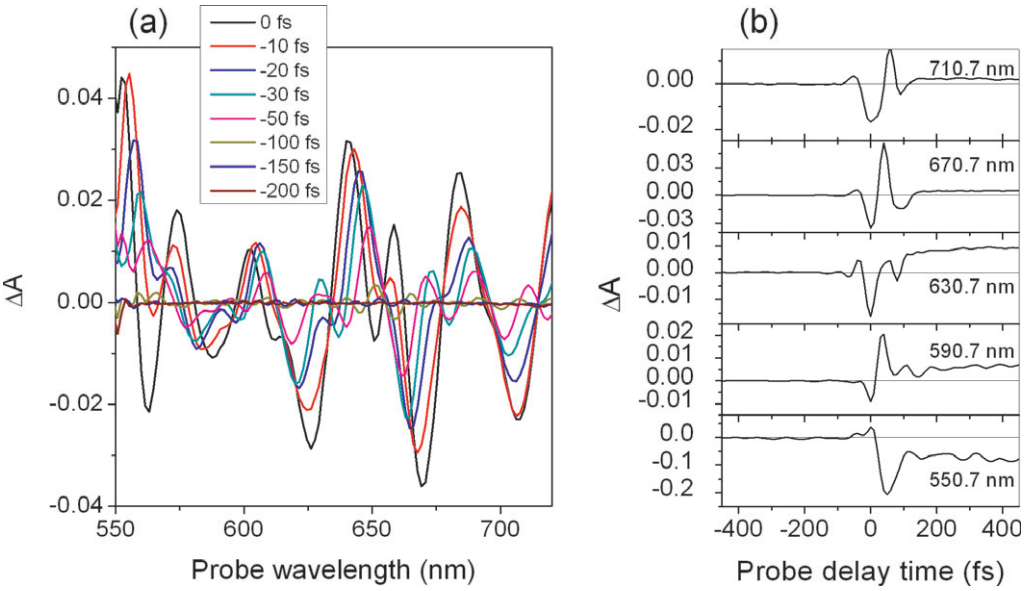

Figure 5. (a) Real-time spectrum at several negative probe delay times. (b) Real-time traces at five different wavelengths in the probe delay time range from −450 to 450 fs.

that the competition between the negative bleaching signal and the tail of the positive-induced absorption results in $A_3(\omega)$ being much smaller than $A_1(\omega)$ and $A_2(\omega)$.

The energy level position is now discussed. From the absorption spectrum shown in figure 1, state S_2^{FE} is estimated to be at 2.25 eV. The energy gap between S_2^{FE} and S_1 is expected to be small. However, the gap is expected to be larger than 200 cm^{-1} corresponding to the room temperature. It is required for the two states to be separated. Otherwise, after relaxation to the 2^1A_g state, it is expected that state S_2^{FE} can be thermally populated, resulting in higher fluorescence quantum efficiency than 10^{-2}. Therefore, state S_1 is estimated as being about 2.2 eV, which is 0.05 eV (400 cm^{-1}) less than 2.25 eV. The energy gap between states S_2 and S_m is estimated as being about 2.15 eV from the peaks of the $A_1(\omega)$ and $A_2(\omega)$ spectra shown in figure 3(d). State S_m is estimated as being ∼4.4 eV. According to the above discussion that the induced absorption band of $2^1A_g \rightarrow nB_u$ is outside the probe spectral range on the shorter wavelength side, the energy gap between 2^1A_g and nB_u is concluded to be ∼2.3 eV. State S_n is thus determined as being ∼4.5 eV.

3.2. Electronic phase relaxation

Figure 5 shows the spectra of absorbance change at the probe photon energy (wavelength) 2.256 to 1.723 eV (550 to 720 nm) from −450 to 0 fs. In this negative pump–probe delay time range, the probing precedes the pumping and the sequence of the field interaction is probe–pump–pump. This is the so-called 'perturbed free-induction decay' sequence and is one of the three orderings of the pump–probe field interaction. The other two sequences are pump–probe–pump, and pump–pump–probe, which are called 'coherent coupling' and 'incoherent population' sequences, respectively [37, 38]. Coherent coupling occurs only when the timings of the pumping and probing overlap with each other, since the condition of two

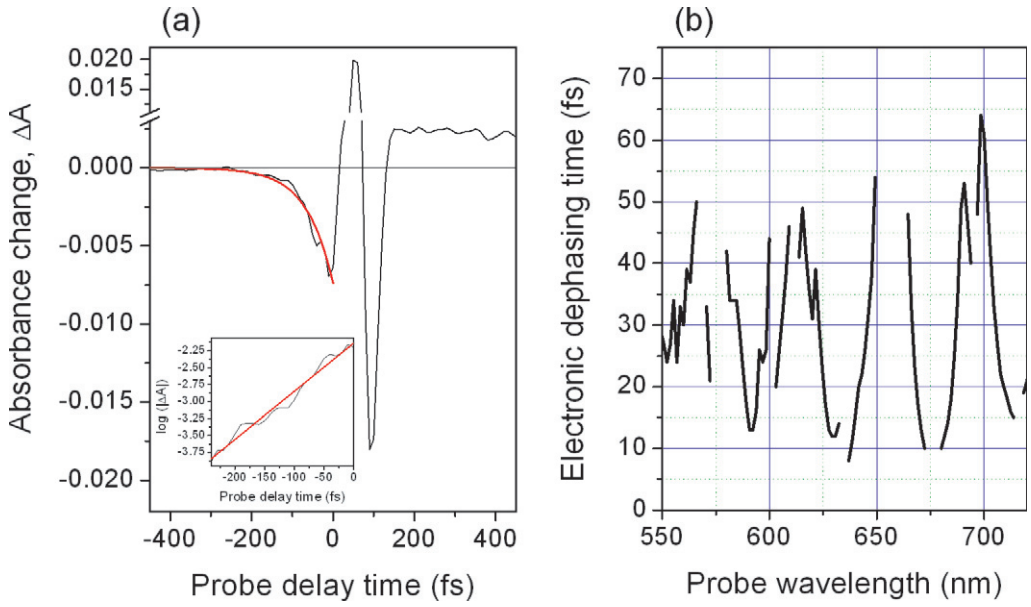

Figure 6. (a) Real-time absorbance change at 698 nm (1.777 eV) in the probe delay time from −450 to 450 fs ($\Delta A(t)$, thin solid line in black) together with the exponential fitting (thick solid line in red) to this trace in the negative probe delay time range. The inset shows the logarithm of the absolute value of absorbance change ($\log|\Delta A(t)|$, black line) and the linear fitting (red line) to it. (b) Electronic dephasing time spectra.

fields from the pump pulse appearing before and after the probe field is such an overlap. An incoherent population arises when the pumping precedes the probing without overlap.

Perturbed free-induction decay is induced by the following mechanism. The preceding probe-pulse generates macroscopic coherent electronic polarization, and the later intense pump field interferes with the probe polarization, resulting in the formation of the grating. Another electric field component of the pump pulse is diffracted by the grating into the direction of the probe pulse. Therefore, the signal disappears when the polarization decays with the dephasing time representing the decay of the electronic coherence between the relevant excited state and the ground state. The signal generated in this process is called perturbed free-induction decay in analogy with free induction decay.

For the 128 probe channels, the real-time traces in the negative probe delay time range were fitted with simple exponential functions. One example is shown in figure 6(a). It shows a good fit to an exponential function. Figure 6(b) shows the probe wavelength dependence of the apparent decay time constants. There are two reasons of the existence of the probe wavelength dependence. The first possible reason is that the perturbed free-induction decay is the process of the relaxation of macroscopic polarization corresponding to the transition between the excited vibronic state and the ground state. The sign of ΔA and its decay time are then dependent on the relevant vibronic state belonging to the same electronic excited state. The second reason is that the signal probably has mixed contributions from a coherent term and perturbed free-induction decay term at negative time. The sum of these two signal contributions can be either constructive or deconstructive depending on the sign of the two signals. The coherent term is given by the

convolution function of the pump and probe pulse without contribution outside of the function. Therefore, the decay in the negative time direction at some wavelengths can be steep owing to the dominant contribution of the coherent term with a minor contribution of the perturbed free-induction decay term, especially when the coherent coupling term has an opposite sign to that of the perturbed free-induction decay term. The apparent lifetime obtained by the exponential fitting may then become much shorter than the real dephasing time. Therefore, the channel with the shortest decay time is considered to contain the largest coherent term contribution and vice versa. As shown in figure 6(b), the measured dephasing time extends from 64 to 9 fs in the spectral range from 550 to 720 nm. It is not reasonable to attribute such a drastic dependence to the different phase relaxation times in such a narrow spectral range. Hence, it is safely attributed to the effect of different contributions of coherent coupling. Therefore, the phase relaxation time between the ground state and the lowest excited state is determined as 64 ± 4 fs, which is the longest time constant shown in figure 6(b).

The probe wavelength dependence of the dephasing time (figure 6(b)) shows several maxima and minima. The averaged spacings between maxima and between minima are 0.124 eV (1000 cm^{-1}) and 0.123 eV (988 cm^{-1}), respectively. This wavelength dependence is probably due to the contribution of coherent spike to the main signal due to the perturbed free-induction decay relevant to the vibronic transition in the negative time range. This is to be discussed elsewhere.

3.3. Vibrational coherent decay time

A Fourier cosine transform was applied to the real-time traces in the probe time range from 0 to 2000 fs. Firstly, the slow electronic relaxation was obtained by removing the vibrational dynamics, which was realized through smoothing the real-time traces by adjacent averaging. Secondly, the vibrational dynamics was obtained by subtracting the slow electronic relaxation from the real-time traces. Thirdly, the fast Fourier cosine transform of the real-time traces in the time range from 0 to 2000 fs was applied, with the results shown in figure 7(a). The peak tracking method [39] was used to obtain the vibrational frequency and amplitude of the peaks around 1460 cm^{-1} as shown in figure 7(a) for each channel. Finally, the probe wavelength dependences of the vibrational amplitude and frequency are plotted in figure 7(a). The frequency of this vibration mode was determined as 1466 cm^{-1} by taking the averaged value of the probe wavelength dependence vibration frequency. In our previous paper, we assigned the vibrational mode observed with a frequency of 1460 cm^{-1} to the wave packet motion in the ground state because of the excitation condition being the stimulated Raman process [40].

The spectral widths in units of wavenumber for this vibration mode were also analyzed for each channel, with the results shown in figure 7(b). From the width of the vibrational modes at a frequency of 1466 cm^{-1}, the vibrational coherent decay times could be calculated. As shown in figure 7(b), all the decay times determined from the FT amplitude spectra are much shorter than the longest probe delay time of 2000 fs in the FT calculation. Therefore, the value of the decay times is not limited by the FT process. The averaged spectral width was determined as 28.1 ± 1.2 cm^{-1} corresponding to the vibrational coherent decay time $\tau_{FT} = 520 \pm 20$ fs. The vibrational coherence decay time of 520 fs is much shorter than the total length of the probe delay time of 20 ps, which is also the reason why the data after the probe delay time of 2000 fs were not used in the FT process. These data hardly contained a clear vibration signal, and their use would introduce a substantial level of noise to the FT results.

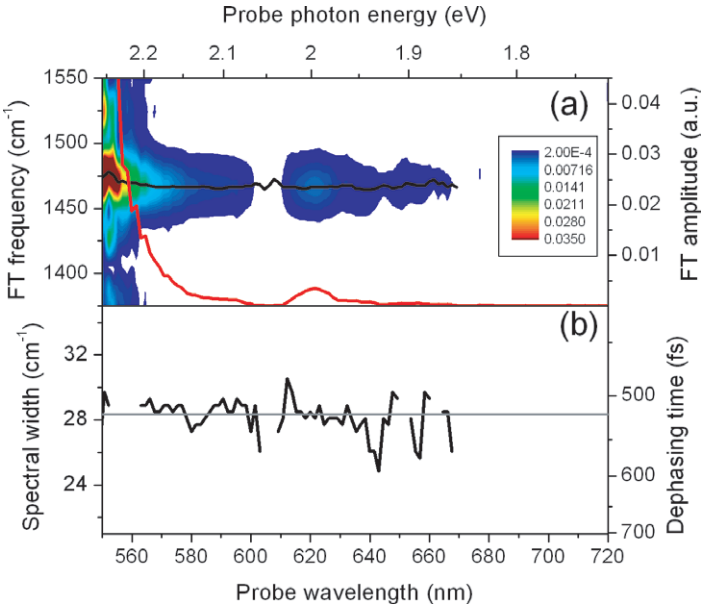

Figure 7. (a) Two-dimension FT amplitude spectrum of the real-time absorbance change ($\Delta A(\omega, t)$), the peak vibrational frequency (black line) and the FT amplitudes of the peaks (red line). (b) Spectral width of the vibrational frequency as a function of probe wavelength (black line). The gray line indicates the dephasing time of 520 fs.

The vibrational dephasing time determined includes both homogeneous (intrinsic dephasing) and inhomogeneous (transition energy distribution) decay contributions, which cannot be separated from each other in principle without invoking a rephasing technique like using photon echoes. To obtain pure dephasing decay free from both electronic and vibrational inhomogeneity, it is necessary to use Raman echoes. The Raman spectrum is expected to contain less electronic inhomogeneity because a monochromatic laser is usually used. This is in contrast to real-time spectroscopy. As shown in the inset of figure 1, the width of the Raman scattering was 15.7 cm^{-1} and it is consistent with the width of the Fourier power spectrum (28.1 cm^{-1}) of the same frequency obtained from the real-time traces. The width of 15.7 cm^{-1} corresponds to a dephasing time of $\tau_{RS} = 940$ fs. The dephasing range is determined from the spectral width as $k = 1/\tau$. In addition, the real vibrational decay time is obtained using $\tau = 1/(k_{FT} - k_{RS})$ as approximately 1160 ± 100 fs.

4. Conclusion

To study electronic and vibronic dynamics together, it is important to conduct an experiment under the same conditions; e.g. the central wavelength, energy and pulse duration of the laser source and the status of sample being studied need to be the same. To realize this objective, real-time vibrational spectral spectroscopy probing both electronic and vibronic dynamics was applied to a quinoid thiophene using a sub-5 fs NOPA laser source. By exponential fitting to the real-time absorbance change of each channel, three relaxation decay times were determined as $\tau_1 = 200$ fs, $\tau_2 = 1.8$ ps and $\tau_3 \gg 20$ ps. They were attributed to the relaxation process

$1^1B_u \xrightarrow{\tau_1} 1^1B_u^* \xrightarrow{\tau_2} 2^1A_g \xrightarrow{\tau_3} 1^1A_g$. The electronic dephasing time was determined as 64 ± 4 fs using the data in the 'negative time' range. The vibrational coherent decay time constant of the strongest coupling mode with a frequency of $1466\,cm^{-1}$ was determined as 520 ± 20 fs from the widths of the corresponding Fourier amplitude spectra.

Acknowledgments

We are grateful to Professor Emeritus Tetsuo Otsubo of Hiroshima University for providing us the sample of Bx-2. This work was partly supported by the grant MOE ATU program in NCTU. A part of this work was performed also under the joint research project of the Laser Engineering, Osaka University under contract subject B1-27.

References

[1] Izumi T, Kobashi S, Takimiya K, Aso Y and Otsubo T 2003 *J. Am. Chem. Soc.* **125** 5286
[2] Pappenfus T M, Chesterfield R J, Frisbie C D, Mann K R, Casado J, Raff J D and Miller L L 2002 *J. Am. Chem. Soc.* **124** 4184
[3] Higuchi H, Nakayama T, Koyama H, Ojima J, Wada T and Sasabe H 1995 *Bull. Chem. Soc. Japan* **68** 2363
[4] Kobayashi T, Yoshizawa M, Stamm U, Taiji M and Hasegawa M 1990 *J. Opt. Soc. Am.* B **7** 1558
[5] Stamm U, Taiji M, Yoshizawa M, Yoshino K and Kobayashi T 1990 *Mol. Cryst. Liq. Cryst.* A **182** 147
[6] Marks R N *et al* 1998 *Chem. Phys.* **227** 49
[7] Muccini M, Lunedei E, Bree A, Horowitz G, Garnier F and Taliani C 1998 *J. Chem. Phys.* **108** 7327
[8] Garnier F, Hajlaoui R, Yassar A and Srivastava P 1994 *Science* **265** 1684
[9] Miller L, Yu Y, Gunic E and Duan R 1995 *Adv. Mater.* **7** 547
[10] Fichou D, Nunzi J-M, Charra F and Pfeffer N 1994 *Adv. Mater.* **6** 64
[11] Furukawa Y, Akimoto M and Harada I 1988 *Synth. Met.* **18** 151
[12] Yang A, Hughes S, Kuroda M, Shiraishi Y and Kobayashi T 1997 *Chem. Phys. Lett.* **280** 475
[13] Heeger A J, Kivelson S, Schrieffer J R and Su W-P 1988 *Rev. Mod. Phys.* **60** 781
[14] Kiess H (ed) 1992 *Conjugated Conducting Polymers* (Berlin: Springer)
[15] Horowitz G, Fichou D, Peng X Z, Xu Z G and Garnier F 1997 *Solid State Commun.* **72** 381
[16] Dodabalapur A, Torsi L and Katz H E 1995 *Science* **268** 270
[17] Noma N, Tsuzuki T and Shirota Y 1995 *Adv. Mater.* **7** 647
[18] Hajlaoui R, Horowitz G and Garnier F 1997 *Adv. Mater* . **9** 389
[19] Geiger F, Stoldt M, Schweizer H, Bauerle P and Umbach E 1993 *Adv. Mater.* **5** 922
[20] Noda T, Ogawa H, Noma N and Shirota Y 1997 *Adv. Mater.* **9** 720
[21] Uchiyama K, Akimichi K, Hotta S, Noge H and Sakaki H 1994 *Synth. Met.* **63** 57
[22] Leclerc M and Faid K 1998 *Handbook of Conduction Polymers* ed T A Skotheim, P K Elsenbaumer and J R Reynolds (New York: Dekker)
[23] Matsuse A, Takeuchi S, Yoshino K and Kobayashi T 1998 *Chem. Phys. Lett.* **288** 165
[24] Yang A, Kuroda M, Shiraishi Y and Kobayashi T 1998 *J. Phys. Chem.* B **102** 3706
[25] Yang A, Kuroda M, Shiraishi Y and Kobayashi T 1998 *J. Chem. Phys.* **109** 8442
[26] Sugita A, Shiraishi Y and Kobayashi T 1998 *Chem. Phys. Lett.* **296** 365
[27] Ozawa A, Takimiya K, Otsubo T and Kobayashi T 2005 *Chem. Phys. Lett.* **409** 224
[28] Wang Z, Otsubo T and Kobayashi T 2006 *Chem. Phys. Lett.* **430** 45
[29] Takahashi T, Matsuoka K, Takimiya K, Otsubo T and Aso Y 2005 *J. Am. Chem. Soc.* **27** 8928
[30] Shirakawa A, Sakane I, Takasaka M and Kobayashi T 1999 *Appl. Phys. Lett.* **74** 2268
[31] Kobayashi T and Shirakawa A 2000 *Appl. Phys.* B **70** S239
[32] Baltuska A, Fuji T and Kobayashi T 2002 *Opt. Lett.* **27** 306

[33] Siebrand W 1966 *J. Chem. Phys.* **44** 4055
[34] Beljonne D, Shuai Z and Bredas J 1992 *J. Chem. Phys.* **98** 8819
[35] Birnbaum D, Fichou D and Kohler B E 1993 *J. Chem. Phys.* **96** 165
[36] Dixit S N, Guo D and Mazumdar S 1991 *Phys. Rev.* B **43** 6781
[37] Mukamel S 1995 *Principle of Nonlinear Optical Spectroscopy* (New York: Oxford University Press)
[38] Brito Cruz C H, Gordon J P, Becker P C, Fork R L and Shank C V 1988 *IEEE J. Quantum Electron.* **24** 261
[39] Yuasa Y, Ikuta M and Kobayashi T 2005 *Phys. Rev.* B **72** 134302
[40] Kobayashi T and Wang Z 2008 *IEEE J. Quantum Electron.* at press